



A Comet Active Beyond the Crystallization Zone

David Jewitt^{1,2}, Man-To Hui¹, Max Mutchler³, Harold Weaver⁴, Jing Li¹, and Jessica Agarwal⁵

¹Department of Earth, Planetary and Space Sciences, University of California, Los Angeles, 595 Charles Young Drive East, Los Angeles, CA 90095-1567, USA; jewitt@ucla.edu

²Department of Physics and Astronomy, University of California, Los Angeles, 430 Portola Plaza, Box 951547, Los Angeles, CA 90095-1547, USA

³Space Telescope Science Institute, 3700 San Martin Drive, Baltimore, MD 21218, USA

⁴The Johns Hopkins University Applied Physics Laboratory, 11100 Johns Hopkins Road, Laurel, MD 20723, USA

⁵Max Planck Institute for Solar System Research, Justus-von-Liebig-Weg 3, D-37077 Göttingen, Germany

Received 2017 August 7; revised 2017 August 24; accepted 2017 August 27; published 2017 September 28

Abstract

We present observations showing inbound long-period comet C/2017 K2 (PANSTARRS) to be active at a record heliocentric distance. Nucleus temperatures are too low (60–70 K) either for water ice to sublimate or for amorphous ice to crystallize, requiring another source for the observed activity. Using the *Hubble Space Telescope* we find a sharply bounded, circularly symmetric dust coma 10^5 km in radius, with a total scattering cross-section of $\sim 10^5$ km². The coma has a logarithmic surface brightness gradient -1 over much of its surface, indicating sustained, steady-state dust production. A lack of clear evidence for the action of solar radiation pressure suggests that the dust particles are large, with a mean size $\gtrsim 0.1$ mm. Using a coma convolution model, we find a limit to the apparent magnitude of the nucleus $V > 25.2$ (absolute magnitude $H > 12.9$). With assumed geometric albedo $p_V = 0.04$, the limit to the nucleus circular equivalent radius is < 9 km. Prediscovery observations from 2013 show that the comet was also active at 23.7 au heliocentric distance. While neither water ice sublimation nor exothermic crystallization can account for the observed distant activity, the measured properties are consistent with activity driven by sublimating supervolatile ices such as CO₂, CO, O₂, and N₂. Survival of supervolatiles at the nucleus surface is likely a result of the comet's recent arrival from the frigid Oort Cloud.

Key words: comets: general – comets: individual (C/2017 K2, Oort Cloud)

1. Introduction

The comets are icy leftovers from planetary accretion and are widely believed to be the most compositionally pristine objects in the solar system. They have survived since formation 4.6 Gyr ago in the Kuiper Belt and Oort Cloud reservoirs, at temperatures below ~ 40 K and ~ 10 K, respectively.

Most known comets are active only when inside the orbit of Jupiter, where sublimation of the most abundant cometary volatile (water ice) is responsible (Whipple 1950). However, activity is occasionally observed in more distant comets (Jewitt 2009; Meech et al. 2009, 2017; Kulyk et al. 2016; Womack et al. 2017) for which numerous explanations have been proposed, most notably the exothermic crystallization of amorphous ice (Priyalnik & Bar-Nun 1990). Other suggestions include reactions of unstable radicals created by prolonged cosmic-ray bombardment (Donn & Urey 1956), polymerization reactions (Rettig et al. 1992), impact (Sekanina 1973), exothermic heat of the solution (Miles 2016), and the sublimation of supervolatile ices (Womack et al. 2017).

In comets observed outbound from perihelion, distant activity has a mundane explanation in terms of the slow propagation of heat acquired at perihelion and conducted into the nucleus interior. For example, the outbound Comet 1P/Halley (perihelion 0.6 au) experienced an outburst at 14 au that was readily explained in this way (Priyalnik & Bar-Nun 1992), as was activity in the outbound comet C/Hale-Bopp at 25 au (Szabó et al. 2011). On the other hand, distant activity in an inbound long-period comet (LPC) cannot be explained by slow conduction, since the comet is approaching the planetary region from larger distances where lower, not higher, temperatures prevail.

Comet C/2017 K2 (PANSTARRS, hereafter K2) was discovered on UT 2017 May 21 (Wainscoat et al. 2017). Its orbit (which, as of 2017 July 24, is a hyperbola with perihelion 1.811 au, semimajor axis -7231 au, eccentricity $e = 1.00025$, and inclination $i = 87^\circ.6$) identifies K2 as an LPC, as does the small Tisserand parameter measured with respect to Jupiter ($T_J \sim 0$; cf. Levison 1996). Perihelion is expected on 2022 December 21. As with other hyperbolic orbit comets, K2 is probably not of interstellar origin, but has been slightly deflected from a bound orbit by planetary perturbations or outgassing forces (Rickman 2014; Dones et al. 2015).⁶ We may thus infer that the surface of the nucleus of K2 is warming from very low temperatures (as small as ~ 10 K in the Oort Cloud) to the current 60 K or 70 K, triggering the observed activity. The initial observations of K2 described here give us an exceptional opportunity to study an Oort Cloud comet as it enters the planetary region.

2. Observations

We secured six images each of 285 s duration using the UVIS mode of the WFC3 camera, under *Hubble Space Telescope* (HST) observing program GO 14939. The WFC3 instrument contains two $2k \times 4k$ charge-coupled device detectors with pixels $0''.04$ on a side, providing a $162'' \times 162''$ field of view from which we read out a $2k$ subarray ($80'' \times 80''$ field). In order to secure maximum signal-to-noise ratio data, we used the extremely broadband F350LP filter: this filter has central wavelength $\lambda_C = 6230$ Å when

⁶ Corrected for planetary perturbations, the pre-entry orbit is parabolic with a semimajor axis of 12,800 au, classifying K2 as dynamically new. See <http://www.oaa.gr.jp/~oaacs/nk/nk3387.htm> by Syuichi Nakano.

Table 1
Observing Geometry

Object	UT Date and Time	r_H^a	Δ^b	α^c	θ_\odot^d	θ_V^e	δ_\oplus^f
CFHT	2013 May 12 14:06–14:28	23.742	23.765	2.4	215.9	354.2	−1.44
<i>HST</i>	2017 Jun 27 20:08–20:48	15.874	15.816	3.7	167.4	357.1	0.52

Notes.

^a Heliocentric distance, in astronomical units.

^b Geocentric distance, in astronomical units.

^c Phase angle, in degrees.

^d Position angle of antisolar direction, in degrees.

^e Position angle of negative projected orbit vector, in degrees.

^f Angle from orbital plane, in degrees.

used on a Sun-like spectrum and has FWHM of 4758 Å. The six images were obtained in two groups of three, dithered on the CCD in order to provide protection against defective pixels. The images were shifted into alignment and combined into a single image of higher signal-to-noise ratio for analysis.

The resulting apparent magnitudes, V , were converted to absolute magnitudes using

$$H = V - 5 \log_{10}(r_H \Delta) - g(\alpha), \quad (1)$$

in which r_H and Δ are the heliocentric and geocentric distances, respectively, and $g(\alpha)$ is a measure of the phase darkening at phase angle α . The phase coefficient is unmeasured; we assume $g(\alpha) = 0.04\alpha$ based on observations of other active comets (Jewitt & Meech 1987a; Meech & Jewitt 1987) but note that the value of $g(\alpha)$ is not critical because the phase angles are small (Table 1).

The effective cross-section for scattering was then calculated from

$$C_d = \frac{1.5 \times 10^6}{p_V} 10^{-0.4H}, \quad (2)$$

where C_d is in km^2 and $p_V = 0.04$ is our assumed value of the V-band geometric albedo. The cross-sections within a set of fixed linear apertures are listed in Table 2.

Prediscovery observations from the Canada–France–Hawaii 3.6 m telescope (CFHT) atop Mauna Kea were identified using the Canadian Astronomy Data Centre archive. The comet was detected in four images taken using the MegaCam prime focus imager ($0''.185$ per pixel) on UT 2013 May 12 and one from May 13. Images from the former date, each of 600 s integration through a U filter ($\lambda_C = 3743 \text{ \AA}$, FWHM = 758 \AA), were shifted according to the motion of the comet and combined into a single 3000 s equivalent composite (Figure 1). The point-spread function (PSF) measured from stars had FWHM = $0''.73$. While the image of K2 is clearly nonstellar, with FWHM = $1''.5 \pm 0''.2$, we were unable to meaningfully determine the surface brightness profile in detail owing to the low signal-to-noise ratio of the CFHT data. The night was photometric to within a few percent. Accordingly, we measured the magnitude of K2 using standard Megacam calibrations but checked the result using photometry of nearby field stars from the USNO-B catalog. Within a $\theta = 2''.3$ radius aperture (linear radius of 40,000 km at the comet), we obtained $U = 23.7 \pm 0.3$. We converted to V using the average color of comets $U - V = 1.15$ (derived from Solontoi et al. 2012 and Jewitt 2015), finding $V = 22.5 \pm 0.5$, where the error bar reflects both noise in the data and our best estimate of the

Table 2
HST Fixed-aperture Photometry^a

Quantity	5	10	20	40	80	160
V [mag] ^b	21.56	20.79	20.02	19.33	18.83	18.66
H [mag] ^c	9.41	8.64	7.87	7.18	6.68	6.51
$C_d/1000$ [km^2] ^d	6.5	13.1	26.7	50.4	79.8	93.3

Notes.

^a Aperture radii in units of 10^3 km at the comet.

^b Mean apparent V magnitude.

^c Absolute V magnitude calculated from Equation (1).

^d Scattering cross-section $\times 10^{-3} \text{ km}^2$ from Equation (2).

possible uncertainty in the color of K2. The corresponding absolute magnitude computed from Equation (1) is $H = 8.6 \pm 0.5$, about 1.4 ± 0.5 mag fainter than the 40,000 km measurement from 2017 (Table 2), albeit with considerable uncertainty.

3. Discussion

The central $\sim 5''$ of the coma appears nearly circularly symmetric in the plane of the sky (Figure 1). A mild asymmetry at larger radii, toward position angle $300^\circ \pm 10^\circ$, is aligned with neither the antisolar direction nor the projected orbit. It presumably reflects a weak anisotropy in the ejection from the nucleus. We searched for near-nucleus azimuthal structures (“jets”) by subtracting annular average brightnesses from the data, but found none.

The surface brightness profile, $\Sigma(\theta)$, computed using circular azimuthal averaging, consists of three parts (Figure 2). In the central region ($\theta < 0''.2$) the profile is affected by convolution with the PSF of *HST* (see below). In the middle region, the radius range $0''.2 \leq \theta \leq 2''$, a least squares power-law fit to the profile, $\Sigma(\theta) \propto \theta^m$, gives the logarithmic gradient $m = -1.01 \pm 0.01$. This is close to the canonical value, $m = -1$, expected for a coma expanding in steady state and is very different from the value, $m = -3/2$, expected from the action of solar radiation pressure on a steady-state coma (Jewitt & Meech 1987b). The absence of evidence for the effects of radiation pressure is strengthened by the lack of the familiar bow-wave-shaped “nose” of the coma in the sunward direction (Figure 1).

In the outer region ($\theta > 2''$, corresponding to 23,000 km at the comet), the gradient progressively steepens, with Σ reaching 1% of the core value at $\theta = 3''.6$ and 0.1% at $\theta = 9''$. The steepening is azimuthally symmetric in the plane of the sky and suggests an edge to the coma, rather than the

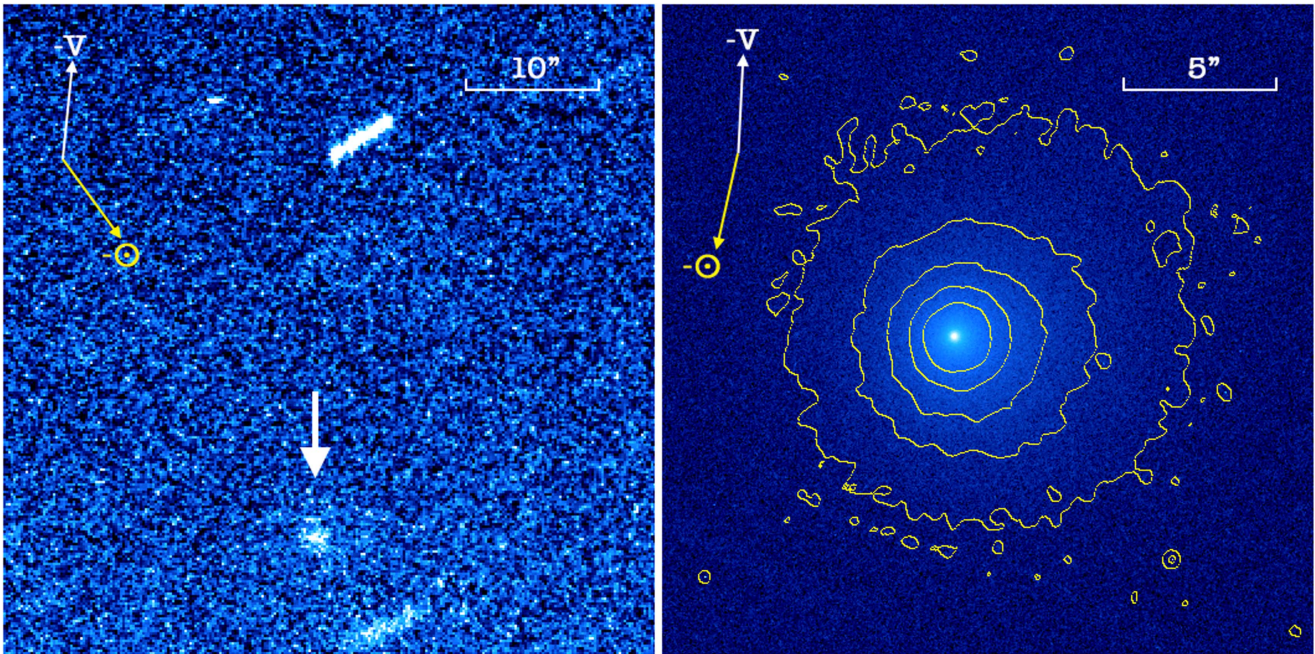


Figure 1. Left: predisccovery CFHT image of C/2017 K2 (arrow) from UT 2013 May 12 at 23.765 au. Right: *HST* image from UT 2017 June 27 at 15.874 au. The antisolar (\ominus) and negative velocity ($-V$) vectors are marked. Both images have north to the top and east to the left).

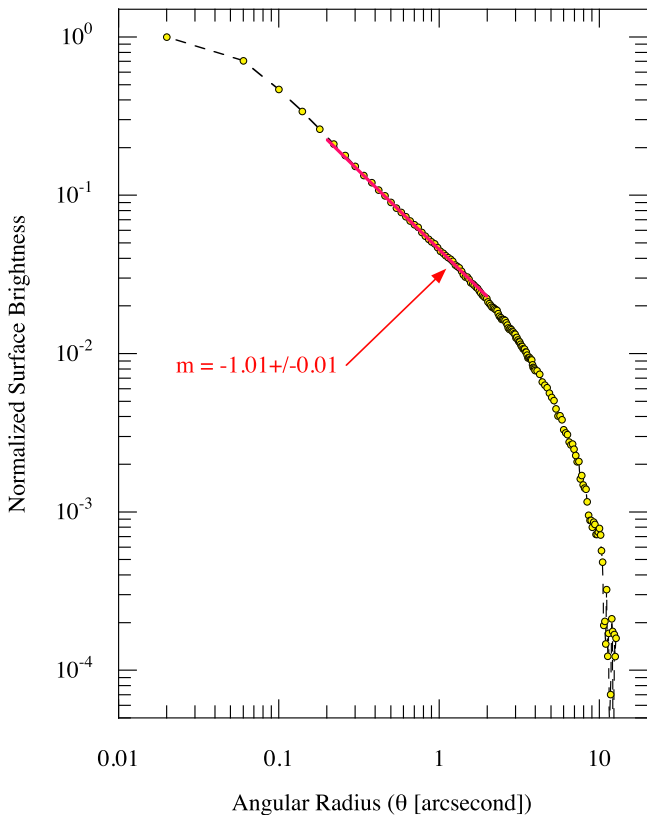


Figure 2. Surface brightness profile determined in annular bins $0''.04$ wide for $\theta < 4''$ and $0''.16$ wide otherwise, with sky subtraction from a surrounding annulus extending from $20''$ to $22''$. The red line segment shows a slope of $m = -1$ and accurately fits the profile in the range $0''.2 \leq \theta \leq 2''.0$.

effects of deflection of dust particle trajectories by radiation pressure. Both the symmetric coma and the steep-edged profile distinguish K2 from many comets reported in the literature (Jewitt & Meech 1987b; Meech et al. 2009; Sárneczky et al.

2016) but do resemble the sharply truncated profile of long-period comet C/1980 E1 (Bowell; Jewitt et al. 1982). Because the sky noise grows substantially at larger radii, we take $\theta = 9''$ as the best estimate of the radius of the coma (corresponding to linear radius $r_c = 1.0 \times 10^8$ m at $\Delta = 15.824$ au).

We attempted to isolate the nucleus of K2 using the surface brightness profile. Photometry using the smallest practical aperture, $0''.2$ in radius, with sky subtraction from a contiguous annulus of outer radius $0''.28$, yielded apparent magnitude $V = 23.27 \pm 0.01$ ($H = 11.02 \pm 0.01$, corresponding to radius $r_n = 22$ km with albedo $p_V = 0.04$). However, given that simple aperture photometry blends light scattered from the nucleus and near-nucleus coma, this must represent a strong upper limit to the possible radius of the nucleus. We sought to better isolate the nucleus by fitting and subtracting a model of the two-dimensional surface brightness of the coma. The model, based on Lamy et al. (2004 and references therein), fits a power-law relation along multiple azimuths within an annulus and then extrapolates the fit to zero radius and convolves with the PSF to model the inner coma. We experimented with a range of fitting radii from $0''.2$ to $0''.4$ at the inner edge to outer radii from $1''.0$ to $2''.0$ (i.e., the power-law portion of the profile in Figure 2). The PSF was obtained from the online TinyTim routine (Biretta 2014). Our best estimate is that the nucleus has a magnitude $V > 25.2$, corresponding to a nucleus absolute magnitude $H > 12.9$. With $p_V = 0.04$, Equation (2) gives the cross-section $C_n < 260$ km². The radius of an equal-area circle is $r_n < 9$ km, which is our best estimate of the size of the nucleus.

The simplest interpretation of the data suggested by the circular isophotes (Figure 1) and by the $m = -1$ surface brightness gradient (Figure 2) is that the coma of K2 is in steady-state expansion (Jewitt & Meech 1987b). If we assume that the earliest observations of activity in K2 (in 2013) correspond to the release of the dust particles, then the timescale of the expansion is $t \sim 10^8$ s, and the mean velocity of the particles over this interval is $v = r_c/t$, or $v = 1$ m s⁻¹.

This is a factor of ~ 100 times smaller than the thermal velocity in gas at the distance of K2. In comets closer to the Sun, low dust speeds are usually associated with larger particles (which are poorly dynamically coupled to the outflowing gas; Agarwal et al. 2016).

The absence of evidence for radiation pressure acceleration independently suggests that the coma dust particles must be large. The radiation pressure induced acceleration is $\beta g_{\odot}(1)/r_H^2$, where r_H is the heliocentric distance expressed in astronomical units, $g_{\odot}(1) = 0.006 \text{ m s}^{-2}$ is the gravitational acceleration to the Sun at $r_H = 1 \text{ au}$, and β is the dimensionless radiation pressure efficiency, approximately equal to the inverse of the grain radius expressed in microns, $\beta \sim a_{\mu\text{m}}^{-1}$ (Bohren & Huffman 1983). Then, the distance of deflection is just $\ell = \beta g_{\odot}(1)t^2/(2r_H^2)$, where t is the time of flight. Substituting $t \sim 10^8 \text{ s}$ we find that micron-sized particles ($\beta = 1$) should travel a distance $\ell \sim 1 \text{ au}$ and should occupy a long tail, which is not observed. The interpretation is compromised somewhat by the viewing geometry (phase angle $\alpha = 4^\circ$ for the *HST* observation), since we can measure the dust distribution only in the plane of the sky. Assuming dust accelerated in the antisolar direction, we substitute $\ell < r_c/(\sin(\alpha))$, from which we obtain $\beta < 10^{-2}$, corresponding to an effective dust radius $a_{\mu\text{m}} \gtrsim 0.1 \text{ mm}$. This large particle size is qualitatively consistent with a model in which small particles are retained by cohesive forces (Gundlach et al. 2015), but is quantitatively inconsistent because their model predicts that no dust of any size can be ejected beyond $r_H \sim 5 \text{ au}$, clearly in violation of our observations.

The mass of the dust particles, considered as spheres of density ρ , is $M_d = 4\rho a C_d/3$. Substituting $a = 0.1 \text{ mm}$, $\rho = 500 \text{ kg m}^{-3}$, and $C_d = 9.3 \times 10^4 \text{ km}^2$ (Table 2), we find $M_d \sim 6 \times 10^9 \text{ kg}$ equal to roughly 10^{-6} of the nucleus mass, if $r_n = 9 \text{ km}$. If spread uniformly over the surface of a spherical nucleus of radius r_n and density ρ , they would form a layer of thickness $\Delta r = a C_d/(3\pi r_n^2)$. For example, with $r_n = 9 \text{ km}$, we find $\Delta r = 1 \text{ cm}$, comparable to the likely diurnal thermal skin depth. If released steadily over the $t \sim 10^8 \text{ s}$ active lifetime of K2, the average mass-loss rate is $dM/dt \sim 60 \text{ kg s}^{-1}$, a remarkable value for a comet beyond Saturn.

We solved the radiative thermal equilibrium equation for H_2O , CO_2 , and CO ices,

$$\frac{L_{\odot}}{4\pi r_H^2}(1 - A) = \chi[\epsilon\sigma T^4 + L(T)f_s(T)], \quad (3)$$

in which L_{\odot} (W) is the luminosity of the Sun, r_H (m) is the heliocentric distance, A is the Bond albedo, ϵ is the emissivity of the body, σ ($\text{W m}^{-2} \text{ K}^{-4}$) is the Stefan–Boltzmann constant, and $L(T)$ (J kg^{-1}) is the latent heat of sublimation of the relevant ice at temperature T (K). Dimensionless parameter χ characterizes the way in which incident heat is deposited over the surface. To explore the range of possible solutions, we consider the limiting cases $\chi = 1$, which describes the highest possible temperatures found at the subsolar point on a non-rotating nucleus and $\chi = 4$, corresponding to the temperature of an isothermal sphere. The quantity f_s ($\text{kg m}^{-2} \text{ s}^{-1}$) is the sought-after mass flux of sublimated ice. The two terms on the right represent power radiated from the surface into space and power used to sublimate ice, while heat conduction into the nucleus interior is neglected. The term on the left represents power absorbed from the Sun. To solve Equation (3) we used

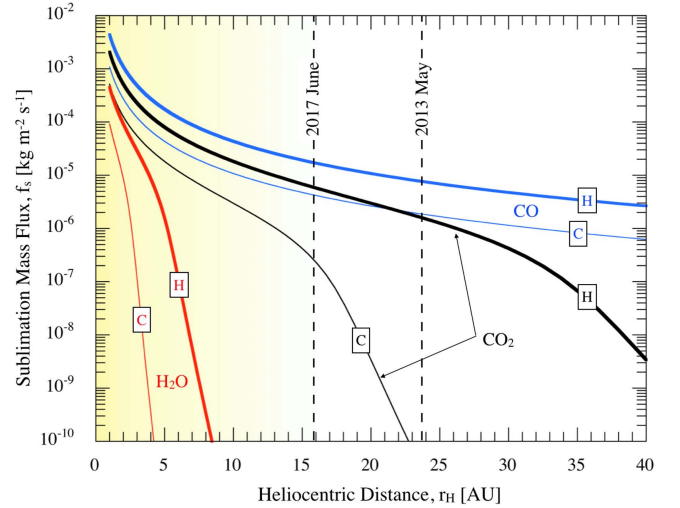


Figure 3. Specific mass sublimation rates as a function of heliocentric distance for three ices of (red) H_2O , (black) CO_2 , and (blue) CO , from Equation (3). The curves for O_2 and N_2 are similar to that for CO and are not plotted for clarity. For each ice, the sublimation rates for the minimum (labeled C for “cold”) and maximum (H for “hot”) possible temperatures are indicated by thin and thick lines, respectively. The shaded region shows the heliocentric distances where crystallization is possible. The heliocentric distances at which the CFHT and *HST* observations were taken are marked by vertical dashed lines.

ice thermodynamic parameters from Brown & Ziegler (1980) and Washburn (1926) and assumed $A = 0.04$, $\epsilon = 0.9$. Solutions to Equation (3) show that sublimation of water ice cannot drive the observed activity of K2 (Figure 3).

The timescale for the crystallization of amorphous ice, τ_{CR} (years), at temperature, T , is

$$\tau_{\text{CR}} = 3 \times 10^{-21} \exp\left(\frac{E_A}{kT}\right), \quad (4)$$

where k is Boltzmann’s constant and $E_A/k = 5370 \text{ K}$ (Schmitt et al. 1989). The comet is infalling on a nearly radial orbit. Accordingly, we estimate the critical distance for the crystallization of surface ice by comparing τ_{CR} with the free-fall timescale, τ_{ff} , given by

$$\tau_{\text{ff}} = \left(\frac{r_H^3}{2GM_{\odot}}\right)^{1/2}, \quad (5)$$

in which G is the gravitational constant and M_{\odot} is the mass of the Sun. We reason that crystallization will occur when $\tau_{\text{CR}} \ll \tau_{\text{ff}}$. Solving Equations (3)–(5) numerically, we find that the inequality is satisfied for the high temperature ($\chi = 1$ in Equation (3)) limit at $r_H \leq 12.5 \text{ au}$ and for the low temperature limit ($\chi = 4$) at $r_H \leq 6.0 \text{ au}$. Both distances are small compared to the heliocentric distance of K2 in the observations discussed here, indicating that crystallization has not occurred. A slightly higher critical distance ($r_H = 16 \text{ au}$) was found for Centaurs by Guilbert-Lepoutre (2012), but this reflects the much longer dynamical timescales for Centaur heating (10 Myr in her integrations compared with $\tau_{\text{ff}} \sim 5 \text{ years}$ here) and is inapplicable to the plunge orbit of K2.

We thus conclude that, unlike other inbound comets that have been studied (Meech et al. 2009, 2017), K2 lies beyond both the water ice sublimation ($r_H \lesssim 5 \text{ au}$) and crystallization ($r_H \leq 12.5 \text{ au}$) zones, ruling out these processes as sources of

the observed activity. Instead, more volatile ices might drive the activity, as shown in Figure 3. For example, at the subsolar point ($\chi = 1$) and at 23.8 au (2013 May), carbon dioxide (latent heat of vaporization $L = 6 \times 10^5 \text{ J kg}^{-1}$) would sublimate at $f_s = 2 \times 10^{-6} \text{ kg m}^{-2} \text{ s}^{-1}$, while the more volatile carbon monoxide, oxygen, and nitrogen ices (all have $L \sim 2 \times 10^5 \text{ J kg}^{-1}$) would sublimate at $f_s = 8 \times 10^{-6} \text{ kg m}^{-2} \text{ s}^{-1}$ (Figure 3). An exposed ice patch having an area $f_s^{-1}(dM/dt) \sim 1\text{--}10 \text{ km}^2$ would be sufficient to supply the mass-loss rate. On a non-rotating, 9 km radius spherical nucleus with a density of 500 kg m^{-3} , these sublimation fluxes are just sufficient to expel particles (of equal density) against gravity, provided their radii are $a \lesssim 0.2 \text{ mm}$ and $a \gtrsim 0.1 \text{ mm}$ particle size inferred from the absence of the radiation pressure deflection of the coma. It is thus plausible that the dust particles in the coma of K2 were launched by gas drag from sublimating supervolatile ices, compatible with limited laboratory evidence for low temperature (40–60 K) sublimation of supervolatile coatings on grains (Bar-Nun et al. 2007). Supervolatiles can also explain the measured brightening in the absolute magnitude from $H = 8.6 \pm 0.5$ at 23.8 au to $H = 7.2$ at 15.9 au. The ratio of equilibrium sublimation rates for CO, O₂, and N₂ at these distances is 2.2:1, corresponding to a brightening by 0.9 mag, while for CO₂ the ratio is 3.8 (1.4 mag), both comparing favorably with the observed 1.4 ± 0.5 mag within the uncertainties. In addition, of the explanations listed in the introduction, supervolatile sublimation is the only one naturally providing sustained (as opposed to burst-like) activity over this extreme distance range. We conclude that supervolatile sublimation is the likely source of the activity in K2.

The emerging picture of K2 is of a <9 km radius nucleus ejecting submillimeter-sized particles at low velocities over periods of years, driven by the sublimation of supervolatile ices. The presence of supervolatile ices in the near-surface regions of the comet is consistent with its long-period orbit and probably dynamically new nature. In this regard, K2 resembles the inbound LPC C/1980 E1 (Bowell), which, at $r_H < 7$ au, displayed a spherical coma with a nearly parallel-sided tail consisting of 0.3–1 millimeter-sized particles of considerable age (Sekanina 1982). The coma expanded linearly at speed $0.9 \pm 0.2 \text{ m s}^{-1}$ in observations over the heliocentric distance range ~ 5.0 au to ~ 3.5 au (Jewitt 1984), similar to the expansion rate of K2. Outgassing of OH from C/1980 E1 only became strong near $r_H = 4.6$ au, apparently caused by sublimation of icy grains in the coma, while the nucleus itself activated only near perihelion (at 3.36 au; A’Hearn et al. 1984). The early detection of K2 (at ~ 24 au versus ~ 7 au for C/1980 E1) will allow a much richer investigation of the behavior of a long-period comet entering the planetary region, leading to an improved understanding of the processes occurring when warming up from Oort Cloud temperatures.

We thank Pedro Lacerda and the anonymous referee for comments. Based on observations made under GO 14939 with the NASA/ESA *Hubble Space Telescope*, obtained at the Space Telescope Science Institute, operated by the Association of Universities for Research in Astronomy, Inc., under NASA contract NAS 5-26555. This research used the facilities of the

Canadian Astronomy Data Centre, National Research Council of Canada with the support of the Canadian Space Agency. D.J. appreciates support from NASA’s Solar System Observations program.

Facility: Hubble Space Telescope.

ORCID iDs

Man-To Hui  <https://orcid.org/0000-0001-9067-7477>
 Max Mutchler  <https://orcid.org/0000-0002-0088-3021>
 Harold Weaver  <https://orcid.org/0000-0003-0951-7762>
 Jing Li  <https://orcid.org/0000-0002-0982-7309>
 Jessica Agarwal  <https://orcid.org/0000-0001-6608-1489>

References

- Agarwal, J., A’Hearn, M. F., Vincent, J.-B., et al. 2016, *MNRAS*, **462**, S78
 A’Hearn, M. F., Schleicher, D. G., Millis, R. L., Feldman, P. D., & Thompson, D. T. 1984, *AJ*, **89**, 579
 Bar-Nun, A., Notesco, G., & Owen, T. 2007, *Icar*, **190**, 655
 Biretta, J. 2014, Space Telescope WFC Instrument Science Report (Baltimore, MD: STScI)
 Bohren, C. F., & Huffman, D. R. 1983, *Absorption and Scattering of Light by Small Particles* (New York: Wiley)
 Brown, G., & Ziegler, W. 1980, *Adv. Cryog. Eng.*, **25**, 662
 Dones, L., Brasser, R., Kaib, N., & Rickman, H. 2015, *SSRv*, **197**, 191
 Donn, B., & Urey, H. C. 1956, *ApJ*, **123**, 339
 Guilbert-Lepoutre, A. 2012, *AJ*, **144**, 97
 Gundlach, B., Blum, J., Keller, H. U., & Skorov, Y. V. 2015, *A&A*, **583**, A12
 Jewitt, D. 1984, *Icar*, **60**, 373
 Jewitt, D. 2009, *AJ*, **137**, 4296
 Jewitt, D. 2015, *AJ*, **150**, 201
 Jewitt, D., Ishiguro, M., Weaver, H., et al. 2014, *AJ*, **147**, 117
 Jewitt, D., & Meech, K. 1987a, *AJ*, **93**, 1542
 Jewitt, D. C., & Meech, K. J. 1987b, *ApJ*, **317**, 992
 Jewitt, D. C., Soifer, B. T., Neugebauer, G., Matthews, K., & Danielson, G. E. 1982, *AJ*, **87**, 1854
 Kulyk, I., Korsun, P., Rousselot, P., Afanasiev, V., & Ivanova, O. 2016, *Icar*, **271**, 314
 Lamy, P. L., Toth, I., Fernandez, Y. R., & Weaver, H. A. 2004, in *Comets II*, ed. M. C. Festou, H. U. Keller, & H. A. Weaver (Tucson, AZ: Univ. Arizona Press), 223
 Levison, H. F. 1996, in *ASP Conf. Ser.* 107, *Completing the Inventory of the Solar System*, ed. T. W. Rettig & J. M. Hahn (San Francisco, CA: ASP), 173
 Meech, K. J., & Jewitt, D. C. 1987, *A&A*, **187**, 585
 Meech, K. J., Pittichová, J., Bar-Nun, A., et al. 2009, *Icar*, **201**, 719
 Meech, K. J., Schambeau, C. A., Sorli, K., et al. 2017, *AJ*, **153**, 206
 Miles, R. 2016, *Icar*, **272**, 356
 Prialnik, D., & Bar-Nun, A. 1990, *ApJ*, **363**, 274
 Prialnik, D., & Bar-Nun, A. 1992, *A&A*, **258**, L9
 Rettig, T. W., Tegler, S. C., Pasto, D. J., & Mumma, M. J. 1992, *ApJ*, **398**, 293
 Rickman, H. 2014, *M&PS*, **49**, 8
 Sárneczky, K., Szabó, G. M., Csák, B., et al. 2016, *AJ*, **152**, 220
 Schmitt, B., Espinasse, S., Grim, R. J. A., Greenberg, J. M., & Klinger, J. 1989, in *ESA Special Publ.* 302, *Physics and Mechanics of Cometary Materials* (Munster: ESA), 65
 Sekanina, Z. 1973, *NASSP*, **319**, 199
 Sekanina, Z. 1982, *AJ*, **87**, 161
 Solontoi, M., Ivezić, Ž., Jurić, M., et al. 2012, *Icar*, **218**, 571
 Szabó, G. M., Sárneczky, K., & Kiss, L. L. 2011, *A&A*, **531**, A11
 Wainscoat, R. J., Wells, L., Micheli, M., & Sato, H. 2017, *CBET*, **4393**
 Washburn, E. 1926, *International Critical Tables of Numerical Data, Physics, Chemistry and Technology*, Vol. 3 (New York: McGraw-Hill)
 Whipple, F. L. 1950, *ApJ*, **111**, 375
 Womack, M., Sarid, G., & Wierzbos, K. 2017, *PASP*, **129**, 031001